J Mater Sci (2016) 51:4150–4159
DOI 10.1007/s10853-016-9738-5

One-step in situ growth of Co_9S_8 on conductive substrate as an efficient counter electrode for dye-sensitized solar cells

Linjie Zheng[1] · Xiaohua Sun[1] · Linlin Chen[1] · Chao Bao[1] · Weilong Luo[1] · Niu Huang[1] · Panpan Sun[1] · Yihua Sun[1] · Liang Fang[2] · Lei Wang[2]

Received: 8 October 2015 / Accepted: 8 January 2016 / Published online: 13 January 2016

Abstract Cobalt sulfide counter electrodes for the dye-sensitized solar cell (DSSC) were successfully prepared on fluorine-doped tin oxide (FTO) glass substrates by a facial one-step in situ solvothermal method. The influences of prepared temperature on the synthesized phase, surface morphology, electrocatalytic, and photovoltaic performances of the cobalt sulfide counter electrodes were investigated with X-ray diffraction (XRD), field-emission scanning electron microscopy (SEM), cyclic voltammetry (CV), electrochemical impedance spectroscopy (EIS), Tafel, and photocurrent density–voltage (*J*–*V*) measurements. The results indicated that very thin Co_9S_8 nanoparticle thin films grew on the FTO substrates and the Co_9S_8 counter electrode prepared at 180 °C showed superior electrocatalytic activity, chemical stability, and photovoltaic performance. The DSSC based on the Co_9S_8 counter electrode prepared at 180 °C exhibited an efficiency of 6.59 % which was comparable to the solar cell based on the sputtering Pt counter electrode (6.82 %). It indicated that Co_9S_8 in situ growing on FTO glass substrate at 180 °C is a potential candidate to replace Pt as a low-cost and efficient counter electrode of DSSC.

✉ Xiaohua Sun
mksxh@163.com

[1] College of Materials and Chemical Engineering, College of Science, Hubei Provincial Collaborative Innovation Center for New Energy Microgrid, China Three Gorges University, Yichang 443002, China

[2] GuangXi Key Laboratory of New Energy and Building Energy Saving, Guilin University of Technology, Guilin 541004, China

Introduction

In the past decades, dye-sensitized solar cells (DSSCs) have attracted considerable attention because of their acceptable efficiencies, low fabrication cost, easy processing, and so on [1–5]. Generally, a typical DSSC includes a dye-sensitized photoanode, an electrolyte with the iodide/triiodine (I^-/I_3^-) redox couple and a catalytic counter electrode (CE). Among these, CE is a significant component of DSSCs, which collects the electrons from the external circuit and catalyzes the reduction of triiodine (I_3^-) to iodine (I^-) between the CE and electrolyte interface [6]. So, the desired CE material should be with high electrical conductivity for the electrons transporting and collecting, high catalytic activity for the reaction of I_3^- to I^- and good stability [7]. At present, noble metal platinum (Pt) is still a judgment criterion in the field of counter electrodes. However, Pt is expensive and scarce. So, it is not a good choice to prepare a large number of Pt CEs for DSSCs. Therefore, it is essential to seek for cost-effective Pt-free CE materials for the future industrial application of DSSCs.

In recent research, various inorganic materials such as transition-metal oxides [8–10], nitrides [11–13], carbides [14–16], sulfides [17–22], and phosphides [23–25] have come into sight. Among them, transition-metal sulfides such as cobalt sulfide have attracted more and more attentions due to their abundant resource, high electrical conductivity, and excellent electrocatalytic activity for the reduction of I_3^-. Xiao et al. [26] prepared original CoS film by the cyclic voltammetry electrodeposition method following a NaHS hydrothermal treatment, and achieved DSSC efficiency of 7.16 %. Jinghao Huo et al. [17] prepared CoS thin film on FTO glass by repetitive electrophoretic deposition and ion exchange deposition, then the thin film was treated with sodium borohydride or/and

sulfuric acid solution. The DSSC based on the treated CoS CE exhibited a power conversion efficiency of 7.72 %. Tai et al. [27] synthesized CNT@$CoS_{1.097}$ nanocomposites by hydrothermal reaction and then deposited it on FTO-coated glasses by using a spray-coating approach, followed by annealing under N_2 atmosphere at different temperatures. The DSSC based on the CNT@Co_9S_8 CE showed a maximum efficiency of 7.78 %. Wang et al. [28] obtained CoS/graphene CE by a one-pot hydrothermal and a doctor blade method, and achieved 7.08 % of the DSSC efficiency. Jin et al. [29] synthesized monodispersed CoS_2 nano-spheres by a hydrothermal method and fabricated CEs by a cast-coating method, finally achieved a DSSC efficiency of 6.78 %. Chen et al. [30, 31] fabricated Co_9S_8 nanoneedle arrays on conducting plastic substrate and FTO substrate by a chemical bath deposition and an ionic-exchange process. They achieved a power conversion efficiency of 5.47 and 3.72 % for flexible dye-sensitized solar cells and quantum dot-sensitized solar cells, respectively. However, the fabrication procedures of these CEs were relatively complicated, which has limited their promotion [32]. In situ growth has been considered to be a very simple and effective method for fabrication of CEs of DSSCs [33].

In this work, we present a simple one-step solvothermal method for in situ preparation of cobalt sulfide thin films on FTO glass substrates without any surfactant. Under the optimum conditions, the prepared Co_9S_8 samples were used directly as the CEs without any post-treatment, expressing a superior electrocatalytic activity and stability. The corresponding DSSC delivered an efficiency of 6.59 %, which was comparable to that of the DSSC based on sputtering noble Pt counter electrode (6.82 %) tested under similar conditions.

Experimental procedure

Materials

Tetrabutyl titanate (TBT), Polyethylene glycol (PEG, MW = 20,000), Triton-X100, ethanol, HNO_3, $LiClO_4$, CH_3COOH, acetonitrile, and propylene Propylene carbonate (PC) were obtained from Sinopharm Chemical Reagent Corporation (China). $Co(CH_3COO)_2.4H_2O$ and thiourea were obtained from Aladdin Industrial Incorporation. Iodine (I_2, 99.8 %) was obtained from Beijing Yili chemicals (China). Lithium iodide (LiI, 99 %) and 4-tert-butylpyridine (TBP) were purchased from Acros. The Ru-dye, cis-di(thiocyanato)-bis(2,2′-bipyridyl-4,4′-dicarboxylate) ruthenium(II) (N719), was purchased from Solaronix (Switzerland). All the reagents used were of analytical purity without further purification. Fluorine-doped SnO_2 conductive glass (FTO) was used as the substrate for the deposition of mesoporous nanocrystalline TiO_2 film and counter electrodes.

Preparation of the cobalt sulfide counter electrode

The transparent FTO glass substrates were ultrasonically cleaned sequentially in deionized water, acetone, and ethanol for 20 min, respectively, and then were stored in ethanol. Cobalt sulfide thin films were directly grown on FTO substrates by one-step solvothermal method. The preparation processes of cobalt sulfide thin films are as follows: $Co(CH_3COO)_2{\cdot}4H_2O$ (2 mmol, Aladdin) and thiourea (2.1 mmol, Aladdin) were dissolved in 35 mL ethanol and stirred until it achieved a clear and homogeneous blue solution. The entire solution was then transferred into a 50 mL Teflon-lined autoclave and a piece of cleaned FTO substrate was placed at an angle against the wall of the Teflon-lined autoclave with the conductive side facing down. The autoclave was sealed and maintained in an oven at 160, 180, and 200 °C for 18 h and then cooled to room temperature naturally. The prepared counter electrodes were washed several times with deionized water and ethanol and then dried in a vacuum oven at 50 °C for 1.5 h. According to their synthesis temperature, they were named as Co_9S_8-160, Co_9S_8-180 and Co_9S_8-200 CEs, respectively.

Fabrication of DSSC

Nanocrystalline TiO_2 paste for fabricating the transparent mesoporous layer of electrode was prepared according to the reported procedure [34]. The prepared TiO_2 paste was coated on the bare fluorine-doped tin oxide (FTO) glass using the doctor blade method. After drying in air, the films were calcined at 500 °C for 30 min. The calcined TiO_2 electrode was preheated at 110 °C for 30 min and then immersed in anhydrous ethanol containing 0.5 mM of Ru-dye (Bu4 N)2[Ru(Hdcbpy)2-(NCS)2] (N719 dye, Solaronix) and kept at 60 °C for 12 h. The dye-sensitized TiO_2 electrodes were rinsed with ethanol and dried in an oven at 70 °C for 30 min. A sandwich-type DSSC was fabricated by the following procedure. One drop of iodine-based electrolyte solution was deposited onto the surface of the TiO_2 photoanode and penetrated inside the TiO_2 film via capillary action. The electrolyte solution was composed of 0.1M1-propy-3-methylimidazolium iodide (PMII), 0.05 M LiI, 0.1 M Guanidinium thiocyanate (GNCS), 0.03 M I_2, and 0.5 M 4-tert-butylpyridine (TBP) in mixed solvent of acetonitrile and propylene carbonate (PC) (volume ratio: 1/1). A platinized FTO counter electrode or a cobalt sulfide counter electrode was then clipped onto the top of the TiO_2 photoanode to form a sandwich-type test cell and then the cell was tested immediately.

Characterization

Morphology of cobalt sulfide counter electrodes was observed with a Sirion FEG field-emission scanning electron microscope (SEM). XRD patterns were recorded on a Rigaku D/max-2500 X-ray diffractometer. The chemical states and compositions of the CEs were characterized by X-ray photoelectron spectroscopy (XPS, Thermo Scientific, Escalab 250Xi). *J–V* characteristics of the DSSCs were measured on the CHI660D electrochemical workstation under AM1.5G simulated solar irradiation (Oriel 91192, USA) with an intensity of 100 mW/cm^2, which was calibrated by a Si photodiode. The active area of solar cells was located at 0.25 cm^2 by employing a metal plate as mask. The electrolyte consisted of 0.6 M 1, 3-dimethylimidazolium iodide, 0.1 M guanidinium thiocyanate, 0.05 M LiI, 0.03 M I_2, and 0.5 M 4-tert-butylpyridine in acetonitrile. Sandwich cells were then prepared by clamping together the TiO_2 photoanode with the counter electrode. Electrochemical impedance spectroscopy (EIS) was carried out with a computer-controlled electrochemical workstation (CHI660D, CH Instruments). The spectra were scanned in a frequency ranging from 0.05 Hz to 100 kHz at room temperature and the magnitude of modulation signal was 0.01 V. The obtained electrochemical impedance spectra were fitted with Z-View software in terms of the appropriate equivalent circuit as shown in Fig. 4. Tafel polarization was also performed for the symmetrical dummy cells with a scan rate of 10 mV/s in dark condition. Cyclic voltammetry (CV) measurements were conducted in a three-electrode system at a scan rate of 50 mV s^{-1}, using Pt-foil as CE, Ag/AgCl as reference electrode, and the as-prepared cobalt sulfide counter electrode as working electrode. The I^-/I_3^- electrolyte consisted of 0.1 M $LiClO_4$, 10 mM LiI, and 1 mM I_2 in acetonitrile.

Results and discussion

Characterization of materials

Figure 1a shows the X-ray diffraction (XRD) patterns of the cobalt sulfide samples growing on FTO glass substrates at different temperatures. Maybe due to the trace amounts or low crystallinity of the samples on FTO glass substrates, no diffraction peaks of cobalt sulfide can be observed obviously, and the prepared counter electrodes show only the diffraction peaks of FTO substrates. In order to confirm the composition of the as-synthesized samples, the corresponding powder samples obtained from in situ solvothermal method also were detected by the XRD as shown in Fig. 1b. All diffraction peaks of the three samples located at 30.06°, 31.36°, 39.67°, 47.57°, 52.23°, 54.58°, 61.34°, and 62.26° match well with those of Co_9S_8 (JCPDS No.86-2273) [35]. However, for sample prepared at 160 °C, there is an unknown diffraction peak existed at 35.55° in its XRD pattern. With increasing the reaction temperature, the crystallinity of samples increased gradually and the unknown diffraction peak faded away.

Figure 2 shows the surface morphology of the cobalt sulfide samples synthesized at 160, 180, and 200 °C for 18 h, respectively, and the cross-sectional SEM image of the cobalt sulfide samples growing on FTO glass substrate at 180 °C for 18 h. It can be seen that cobalt sulfide samples are nanoparticle thin films and the Co_9S_8-180 sample

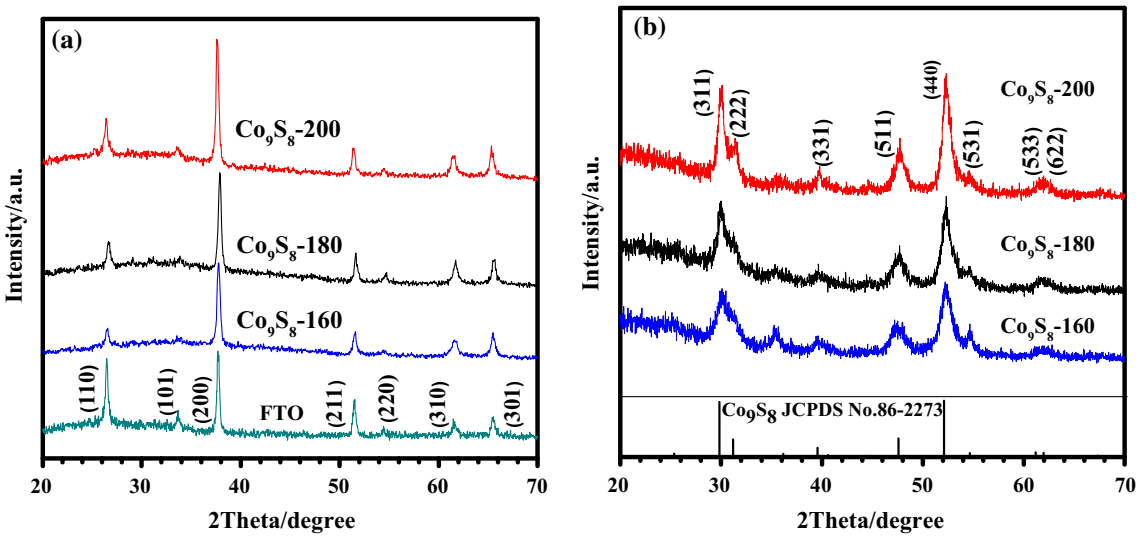

Fig. 1 X-ray diffraction patterns of the cobalt sulfide samples growing on FTO glass substrates at different temperatures (**a**) and that of the corresponding powder samples obtained from in situ solvothermal method (**b**)

shows some large particles aggregated by lots of nanoparticles, which makes film surface rough. The surface of Co_9S_8-200 sample is relatively compact and smooth. High surface roughness can support a high surface area of the CE, which is benefit for enhancing the electrocatalytic activity of the CE [36]. Co_9S_8-180 CE shows a relatively high surface roughness and maybe has a relatively large surface area. Unfortunately, we could not get the data for surface areas because the films were too thin to meet the lowest requirement in the BET tests. In addition, it can be seen from Fig. 2d that very thin cobalt sulfide thin film grows on the FTO thin film. The thickness of cobalt sulfide thin film was found to be about 130 nm.

The full and high-resolution XPS spectra of the cobalt sulfide sample growing on FTO glass substrate at 180 °C are shown in Fig. 3, which was used to further analyze the surface composition and oxidation states of the elements. It confirms the presence of Co and S signals. In the Co 2p and S 2p high-resolution spectra (as shown in Fig. 3b, c), the Co 2p3/2 peak at 778.5 eV and the S 2p3/2 peak at 163.1 eV are matched well with the XPS spectral characteristic of Co_9S_8 [30, 37–39]. In addition, there is a peak at 777.8 eV in the Co 2p spectrum, which corresponds to the Co 2p3/2 peak of the Co, and there is a main peak at 164.25 eV in the S 2p spectrum, which is assigned to the S 2p3/2 peak of S_8 [39]. It is reasonable to presume that Co_9S_8 with some amorphous cobalt sulfide phase was formed on FTO glass substrate. This result is in accordance with XRD analysis.

Electrochemical properties of CEs

In order to investigate the electrocatalytic activity of the CEs, EIS measurements were performed in a symmetrical dummy cell constructed with two identical CEs (CE/electrolyte/CE). The typical Nyquist plots and the equivalent circuit are shown in Fig. 4. A semicircle can be observed in the high-frequency region for all the CEs. It reflects the charge-transfer resistance ($R_{ct\text{-}EIS}$) which is mainly related to the electrocatalytic activity for triiodine reduction at the CE/electrolyte interface [40]. The intercept of the semicircle on the real axis presents the ohmic series resistance (R_s). Apart from the external wires, clips, and size of the FTO glass, conductivity of CE also has a significant effect on R_s [41, 42]. The right arc in the low frequency is ascribed to the Nernst diffusion resistance (Z_w) of the redox couple in the electrolyte [43]. The insert shows the equivalent circuit diagram of EIS containing a constant phase element (CPE), which is the double-layer capacitance at the CE/electrolyte interface. All the Nyquist plots were fitted using Z-view software according to the equivalent circuit, and the fitted parameters are summarized in Table 1. It is noticed that Pt CE has lower R_s than Co_9S_8-based CEs, which demonstrates that Pt CE still has better

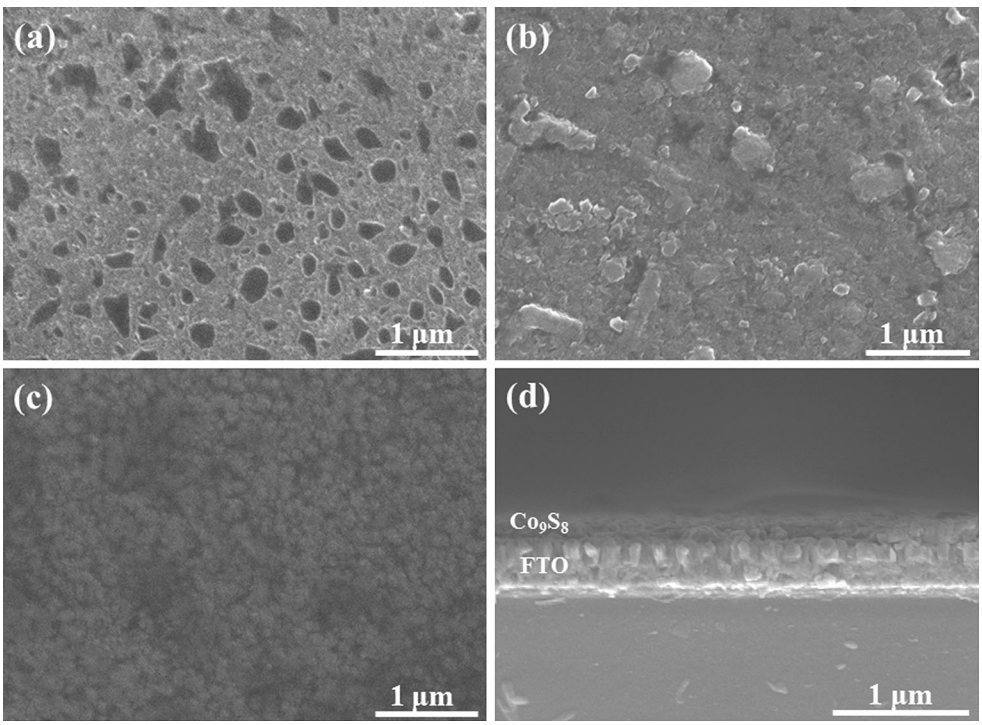

Fig. 2 The surface morphology of the cobalt sulfide samples synthesized at **a** 160, **b** 180, and **c** 200 °C for 18 h, respectively, and **d** the cross-sectional SEM image of the cobalt sulfide sample growing on FTO glass substrate at 180 °C for 18 h

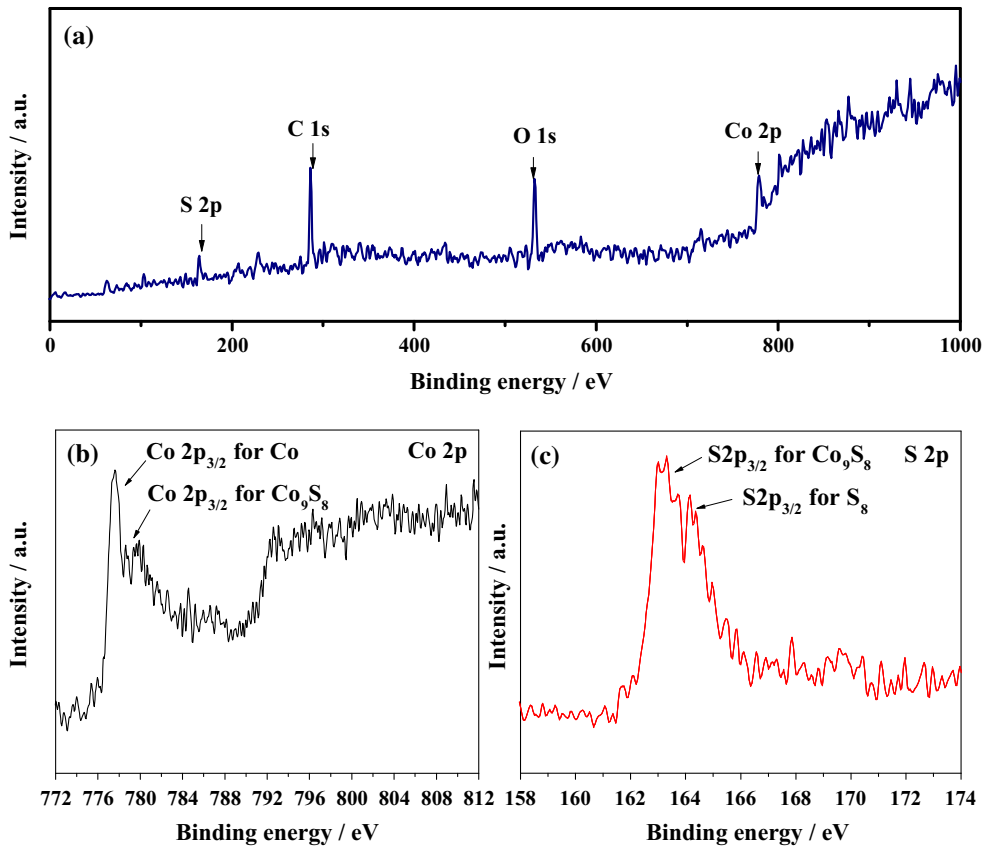

Fig. 3 The full and high-resolution XPS spectra of the cobalt sulfide growing on FTO glass substrate at 180 °C for 18 h

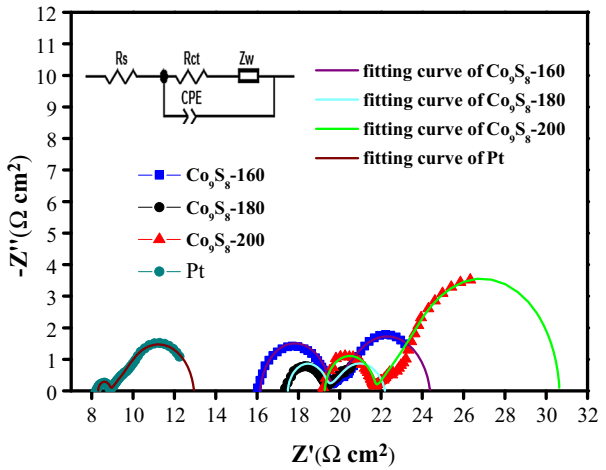

Fig. 4 Nyquist plots and fitting curves of the symmetrical dummy cell constructed with two identical Pt and Co_9S_8-based CEs (Color figure online)

conductivity. The $R_{ct\text{-}EIS}$ is an index to indicate the electrocatalytic performance of the CE. The lower $R_{ct\text{-}EIS}$ represents the higher catalytic performance of the CE [26, 44, 45]. The $R_{ct\text{-}EIS}$ value of the Co_9S_8-180 CE is 1.849 Ω cm^2, which is higher than that of the Pt CE (0.573 Ω cm^2), but lower than that of other two Co_9S_8-based CEs. It indicates that Co_9S_8-180 CE has the highest electrocatalytic activity among the Co_9S_8-based CEs. Meanwhile, Co_9S_8-180 CE has the lowest Nernst diffusion resistance (Z_w) among four CEs (including Pt CE), i.e., iodine ion's transport is the fastest in the electrolyte for Co_9S_8 device. Fast iodine ion's transport can accelerate reducing dye and is beneficial for improving photovoltaic performance of DSSC. The sum (R_{sum}) of R_s, $R_{ct\text{-}EIS}$ and Z_w is a part of whole series resistance of DSSC (including anode, counter electrode, and electrolyte) [45–47]. On the basis of the same anodes, the smaller the R_{sum}, the larger the fill factor (FF) of the solar cell. So, the FF of Co_9S_8-180 device is larger than that of other Co_9S_8-based devices and smaller than that of Pt-based device (as shown in Table 2). In addition, a larger CPE of the CE corresponds to its larger surface area [26, 36]. The Co_9S_8-180 CE shows the highest CPE value, which is in accordance with the results of the SEM.

The Tafel polarization was used to further explain the catalytic activity of the counter electrodes. Figure 5 shows the Tafel polarization curves of the Pt and Co_9S_8-based CEs. Generally, the curve is divided into three zones: polarization zone, Tafel zone, and limiting diffusion zone according to the potential [48]. Theoretically, the curve at

Table 1 Impedance and electrocatalytic parameters of the symmetrical dummy cells determined by fitting the experimental data according to the equivalent circuit model (as shown in Fig. 4) and the Tafel polarization curves (as shown in Fig. 5)

Sample	R_s (Ω cm^2)	$R_{ct\text{-}EIS}$ (Ω cm^2)	Z_w (Ω cm^2)	R_{sum} (Ω cm^2)	CPE (F cm^{-2})	$R_{ct\text{-}Tafel}$ (Ω cm^2)	$D \times 10^{-6}$ (cm^2 s^{-1})
Co_9S_8-160	16.15	3.311	4.91	24.831	3.9533×10^{-5}	5.113	1.039
Co_9S_8-180	17.49	1.849	2.86	22.199	4.9325×10^{-5}	3.621	1.434
Co_9S_8-200	19.26	2.432	8.91	30.602	3.1142×10^{-5}	4.062	0.770
Pt	8.31	0.573	4.08	12.963	4.008×10^{-5}	2.684	1.166

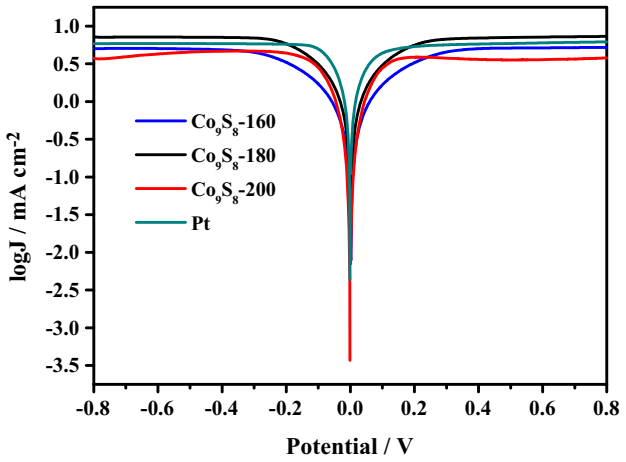

Fig. 5 Tafel curves of the symmetrical dummy cell constructed with two identical Pt and Co_9S_8-based CEs (Color figure online)

relatively low potential but higher than 0.1 V corresponds to the Tafel zone. The information on the exchange current density (J_0) at this region can be obtained. The value of J_0 is the intersection point of the cathodic branch part linear extrapolation and a line perpendicular to the point of zero potential. The steeper the curve in the Tafel zone is, the higher the J_0 is, and the better electrocatalytic activity the CE has [49]. As shown in Fig. 5, the Pt CE displays the highest J_0, followed by the Co_9S_8-180, Co_9S_8-200, and Co_9S_8-160 CEs. This reveals that Co_9S_8-180 CE has the highest electrocatalytic activity among the Co_9S_8-based CEs. The value of exchange current density (J_0) is the kinetic component directly correlated with the electrochemical reaction rate constant and inversely proportional to the charge-transfer resistance ($R_{ct\text{-}Tafel}$), which can be estimated by Eq. (1):

$$J_0 = RT/nFR_{ct-Tafel}, \quad (1)$$

where R is the gas constant, T is the absolute temperature, F is the Faraday constant, and n represents the number of electrons involved in the reduction of I_3^- at the electrode ($n = 2$). The values of $R_{ct\text{-}Tafel}$ calculated according above equation are listed in Table 1. The variation tendency of $R_{ct\text{-}Tafel}$ for all CEs coincides well with that of $R_{ct\text{-}EIS}$ obtained from electrochemical impedance spectroscopy (EIS).

Table 2 Photovoltaic performance data of DSSCs based on different counter electrodes

Sample	J_{sc} (mA cm^{-2})	V_{oc} (V)	FF	η (%)
Co_9S_8-160	13.32	0.70	0.592	5.52
Co_9S_8-180	13.8	0.71	0.663	6.59
Co_9S_8-200	13.57	0.72	0.585	5.72
Pt	14.56	0.70	0.675	6.88

At the diffusion zone, the curves were caused by transport of I_3^- and I^- in the electrolyte. The limiting diffusion current density (J_{lim}) could also be obtained from the curve in this region. The intersection point of the cathodic branch and Y axis is lgJ_{lim}, which can be expressed by Eq. (2):

$$J_{lim} = 2nFCD/l, \quad (2)$$

where C is the I^-/I_3^- concentration, D is the diffusion coefficient of the I_3^- in electrolyte, and l is the spacer thickness. J_{lim} is determined by the diffusion coefficient of the redox couple in electrolyte and also reflects the electrocatalytic activity of the electrode. The values of diffusion coefficient (D) were calculated from above equation and listed in Table 1. It can be noticed that the D values were highly related to the Z_w values obtained from the EIS analysis, i.e., the larger the D, the smaller the Z_w. According to Eq. (2), larger J_{lim} make counter electrodes have larger D (i.e., smaller Z_w) [17]. From Fig. 5, the order of J_{lim} is Pt > Co_9S_8-180 > Co_9S_8-160 > Co_9S_8-200, which is consistent with the decreasing trend of Z_w (as listed in Table 1).

Figure 6 shows the cyclic voltammetry (CV) curves of Pt and Co_9S_8-based CEs. All the electrodes exhibit two pairs of redox peaks. The left peaks are corresponding to the redox reaction between I^- and I_3^-, which directly affects the DSSC performance, while the right peaks are attributed to the redox reaction between I_2 and I_3^-, which has little effect on the DSSC performance [26]. The peak current density (Jpc) and the peak separation between the

anodic and cathodic peaks (Epp) in cyclic voltammetry curves are two significant parameters for comparing catalytic activities of different CEs. The larger |Jpc| value means the fast catalytic reaction speed, and the smaller Epp value means the smaller overpotential for the catalytic reaction [50]. As shown in Fig. 6, the Pt CE has the highest peak current density and the Co_9S_8-180 CE is the best one among all the Co_9S_8-based CEs, which should be attributed to their higher electrocatalytic activity (i.e., smaller Rct) and larger surface area (i.e., bigger CPE value) [36]. It is consistent with the results of EIS and SEM analysis. In addition, the Co_9S_8-based CEs possess similar Epp with the Pt CE, suggesting a similar electrocatalytic process on these electrodes.

Figure 7a presents the CV curves of the Co_9S_8-180 CE in the I_3^-/I^- electrolyte at different scan rates. It can be seen that the cathodic and anodic peaks gradually and regularly shifted negatively and positively,respectively, with the increase of scanning rate gradually. At the same time, anodic and cathodic peak current densities absolute values increase gradually with the increase of scanning speed. Figure 7b illustrates a good linear relationship between anodic and cathodic peaks current densities and the square root of the scan rate for the Co_9S_8-180 counter electrode. This phenomenon demonstrates that there is no species interaction between the I_3^-/I^- redox couple and the Co_9S_8-180 counter electrode. It is only a diffusion-limited process on the Co_9S_8-based counter electrodes [36, 51].

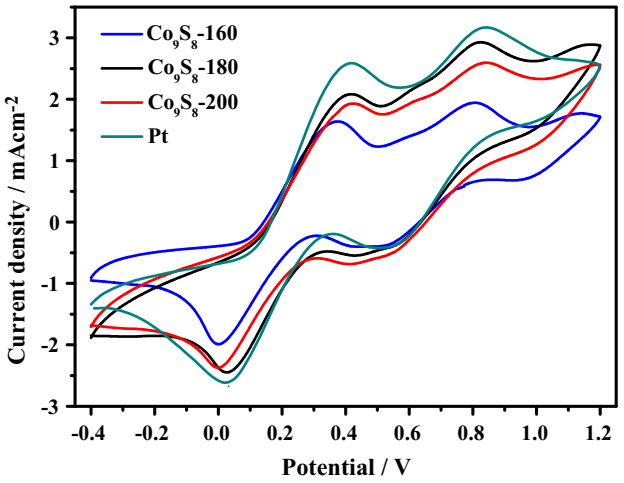

Fig. 6 CV curves of Pt CE and different Co_9S_8-based CEs at the scan rate of 50 mV/s (Color figure online)

The stability of Co_9S_8-180 CE

Long-term stability is an important factor for device industrialization. Figure 8 shows 100 consecutive CV measurements of the CoS-180 counter electrode and the relationship between the number of cyclic scan and the anodic and cathodic peak current densities at the scan rate of 50 mV/s. It can be seen that there is only a slight change from the 1st to 100th scan, indicating that the Co_9S_8-180 counter electrode is tightly bound to the FTO glass substrate and possess fine electrochemical stability in the I^-/I_3^- system [44].

Photovoltaic performances of the cells

The photocurrent density–voltage (*J–V*) curves of DSSCs based on Pt and fabricated Co_9S_8-based counter electrodes are shown in Fig. 9. The corresponding photovoltaic performance parameters are summarized in Table 2. It can be seen that, for the highest electrocatalytic activity, the DSSC based on the Pt CE shows the best photovoltaic

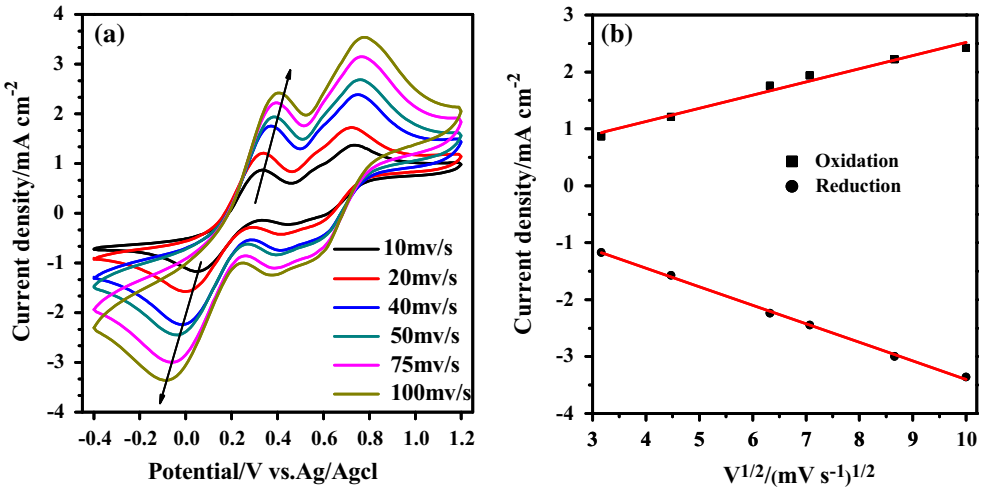

Fig. 7 **a** CV curves of Co_9S_8-180 counter electrode at different scan rates; **b** Linear relationship between cathodic and anodic peak current densities and the square root of scanning speed for Co_9S_8-180 electrode (Color figure online)

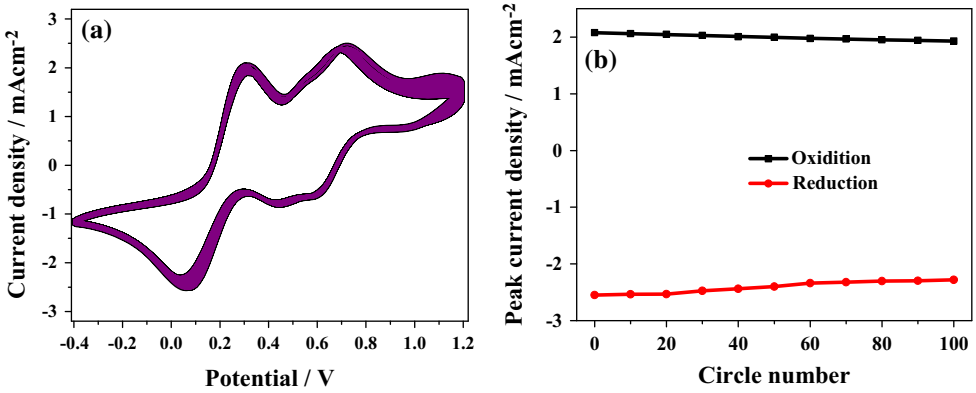

Fig. 8 Consecutive 100 CVs **a** of I_3^-/I^- system for Co_9S_8-180 CE at a scan rate of 50 mV/s, and the relationship **b** between the number of scans and the resultant redox peak current from Fig. 8a

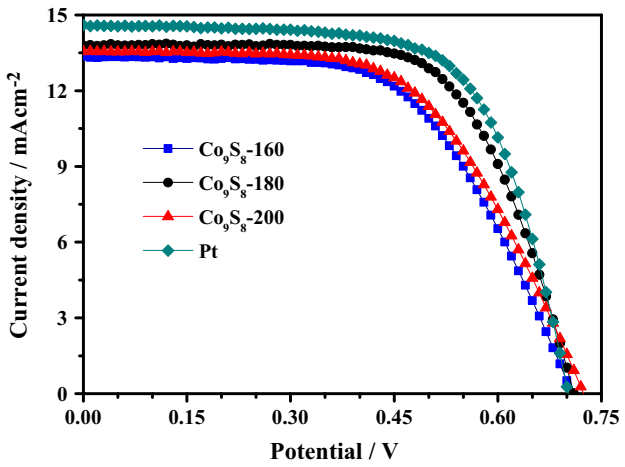

Fig. 9 Photocurrent density–voltage (*J–V*) curves of DSSCs based on Pt and Co_9S_8-based CEs at AM 1.5 irradiation of 100 mW/cm^2

performances with a short-circuit current density (J_{sc}) of 14.56 mA/cm^2, open-circuit voltage (V_{oc}) of 0.7 V, fill factor (FF) of 0.675, and photovoltaic conversion efficiency (η) of 6.88 %. Among all the Co_9S_8-based CEs, the DSSC based on the Co_9S_8-180 CE obtained the highest energy conversion efficiency due to improving the J_{sc} and FF value. The improvement in J_{sc} for the Co_9S_8-180 CE results from its high exchange current density, cathodic peak current density (i.e., high electrocatalytic activity), and high limiting diffusion current density (i.e., fast iodine ion's transport in the electrolyte) [52], as indicated in the Tafel and CV tests. The increase in FF can be attributed to the low R_{sum} (i.e., the sum of R_s, R_{ct}, and Z_w), as discussed in EIS test. Therefore, the DSSC based on the Co_9S_8-180 counter electrode reaches power conversion efficiency of 6.59 %, which is comparable to that of Pt counter electrode (6.88 %) and is 19.4 % higher than that of the DSSC based on Co_9S_8-160 counter electrode. It indicates that cobalt sulfide in situ growing on FTO glass substrate at 180 °C is a potential candidate to replace Pt as a low-cost and efficient counter electrode of DSSC.

Conclusion

In this study, the Co_9S_8 counter electrodes were successfully prepared by a facial one-step in situ solvothermal growth method. The influences of prepared temperature on the synthesized phase, electrocatalytic, and photovoltaic performances of the Co_9S_8-based CEs were investigated. The cobalt sulfide counter electrode prepared at 180 °C showed the highest electrocatalytic activity, good chemical stability, and photovoltaic performance among the Co_9S_8-based CEs. The DSSC based on the Co_9S_8-180 CE achieved the maximum PCE (6.59 %) with a J_{sc} of 13.8 mA cm^{-2}, V_{oc} of 0.71 V, and FF of 0.663, which is very close to that of the DSSC based on the Pt counter electrode (6.82 %). For mild and facile one-step in situ solvothermal method, low-cost counter electrode material, and superior electrocatalytic activity, the Co_9S_8-180 CE is a potential candidate to replace Pt as a low-cost and efficient counter electrode of DSSC.

Acknowledgements This work was supported by the Natural Science Foundation of Hubei Province (Grant No. 2015CFB513), the Research Foundation of Yichang Science and Technology Bureau, China (Grant No. A15-302-a10), Foundation of Key Laboratory of new building energy and building efficiency, Guangxi Province, China (Grant No. 15-J-22-2), and the Foundation of Key Laboratory for UV-Emitting Materials and Technology of Ministry of Education (Grant No. 130026504).

Compliance with ethical standards

Conflict of interest All the authors declare that they have no conflict of interest.

References

1. Peng S, Zhang T, Li L, Shen C, Cheng F, Srinivasan M, Yan Q, Ramakrishna S, Chen J (2015) 3D Cu-doped CoS porous nanosheet films as superior counterelectrodes for quantum dot-sensitized solar cells. Nano Energy 16:163–172
2. Sun X, Zhang Q, Liu Y, Huang N, Sun P, Peng T, Peng T, Zhao X-Z (2014) Photovoltaic performance improvement of dye-

sensitized solar cells through introducing In-doped TiO_2 film at conducting glass and mesoporous TiO_2 interface as an efficient compact layer. Electrochim Acta 129:276–282
3. Kim H-J, Kim C-W, Punnoose D, Gopi CVVM, Kim S-K, Prabakar K, Rao SS (2015) Nickel doped cobalt sulfide as a high performance counter electrode for dye-sensitized solar cells. Appl Surf Sci 328:78–85
4. Sun X, Zhou X, Xu Y, Sun P, Huang N, Sun Y (2015) Mixed P25 nanoparticles and large rutile particles as a top scattering layer to enhance performance of nanocrystalline TiO_2 based dye-sensitized solar cells. Appl Surf Sci 337:188–194
5. Ghani S, Sharif R, Shahzadi S, Zafar N, Anwar AW, Ashraf A, Zaidi AA, Kamboh AH, Bashir S (2014) Simple and inexpensive electrodeposited silver/polyaniline composite counter electrodes for dye-sensitized solar cells. J Mater Sci 50:1469–1477. doi:10.1007/s10853-014-8708-z
6. Wu M, Lin X, Wang Y, Wang L, Guo W, Qi D, Peng X, Hagfeldt A, Gratzel M, Ma T (2012) Economical Pt-free catalysts for counter electrodes of dye-sensitized solar cells. J Am Chem Soc 134:3419–3428
7. Yun S, Hagfeldt A, Ma T (2014) Pt-free counter electrode for dye-sensitized solar cells with high efficiency. Adv Mater 26:6210–6237
8. Sun W, Sun X, Peng T, Liu Y, Zhu H, Guo S, Zhao X-Z (2012) A low cost mesoporous carbon/SnO_2/TiO_2 nanocomposite counter electrode for dye-sensitized solar cells. J Power Sources 201:402–407
9. Wu M, Lin X, Guo W, Wang Y, Chu L, Ma T, Wu K (2013) Great improvement of catalytic activity of oxide counter electrodes fabricated in N_2 atmosphere for dye-sensitized solar cells. Chem Commun 49:1058–1060
10. Wu M, Lin X, Hagfeldt A, Ma T (2011) A novel catalyst of WO_2 nanorod for the counter electrode of dye-sensitized solar cells. Chem Commun 47:4535–4537
11. Li GR, Song J, Pan GL, Gao XP (2011) Highly Pt-like electrocatalytic activity of transition metal nitrides for dye-sensitized solar cells. Energy Environ Sci 4:1680–1683
12. Li GR, Wang F, Song J, Xiong FY, Gao XP (2012) TiN-conductive carbon black composite as counter electrode for dye-sensitized solar cells. Electrochim Acta 65:216–220
13. Li GR, Wang F, Jiang QW, Gao XP, Shen PW (2010) Carbon nanotubes with titanium nitride as a low-cost counter-electrode material for dye-sensitized solar cells. Angew Chem Int Edit 49:3653–3656
14. Liao Y, Pan K, Wang L, Pan Q, Zhou W, Miao X, Jiang B, Tian C, Tian G, Wang G, Fu H (2013) Facile synthesis of high-crystallinity graphitic carbon/FeC nanocomposites as counter electrodes for high-efficiency dye-sensitized solar cells. ACS Appl Mater Interfaces 5(9):3663–3670
15. Wu M, Lin X, Hagfeldt A, Ma T (2011) Low-cost molybdenum carbide and tungsten carbide counter electrodes for dye-sensitized solar cells. Angew Chem Int Ed Engl 50:3520–3524
16. Vijayakumar P, Senthil Pandian M, Lim SP, Pandikumar A, Huang NM, Mukhopadhyay S, Ramasamy P (2015) Investigations of tungsten carbide nanostructures treated with different temperatures as counter electrodes for dye sensitized solar cells (DSSC) applications. J Mater Sci 26:7977–7986. doi:10.1007/s10854-015-3452-y
17. Huo J, Zheng M, Tu Y, Wu J, Hu L, Dai S (2015) A high performance cobalt sulfide counter electrode for dye-sensitized solar cells. Electrochim Acta 159:166–173
18. Geng H, Zhu L, Li W, Liu H, Quan L, Xi F, Su X (2015) FeS/nickel foam as stable and efficient counter electrode material for quantum dot sensitized solar cells. J Power Sources 281:204–210
19. Zhang Y, Shi C, Dai X, Liu F, Fang X, Zhu J (2014) Pyrolysis preparation of Cu_2ZnSnS_4 thin film and its application to counter electrode in quantum dot-sensitized solar cells. Electrochim Acta 118:41–44
20. Yan X, Tong X, Ma L, Tian Y, Cai Y, Gong C, Zhang M, Liang L (2014) Synthesis of porous NiS nanoflake arrays by ion exchange reaction from NiO and their high performance supercapacitor properties. Mater Lett 124:133–136
21. Jia J, Wu J, Dong J, Zhou P, Wu S, Lin J (2015) Cobalt selenide/tin selenide hybrid used as a high efficient counter electrode for dye-sensitized solar cells. J Mater Sci 26(12):10102. doi:10.1007/s10854-015-3694-8
22. Dong J, Wu J, Zheng M, Huo J, Tu Y, Lan Z (2015) Petal-like cobalt selenide nanosheets used as counter electrode in high efficient dye-sensitized solar cells. J Mater Sci 26:2501–2507. doi:10.1007/s10854-015-2713-0
23. Dou YY, Li GR, Song J, Gao XP (2012) Nickel phosphide-embedded graphene as counter electrode for dye-sensitized solar cells. Phys Chem Chem Phys 14:1339–1342
24. Wu M, Bai J, Wang Y, Wang A, Lin X, Wang L, Shen Y, Wang Z, Hagfeldt A, Ma T (2012) High-performance phosphide/carbon counter electrode for both iodide and organic redox couples in dye-sensitized solar cells. J Mater Chem 22:11121
25. Wu MS, Wu JF (2013) Pulse-reverse electrodeposition of transparent nickel phosphide film with porous nanospheres as a cost-effective counter electrode for dye-sensitized solar cells. Chem Commun 49(93):10971–10973
26. Xiao Y, Han G, Chang Y, Zhang Y, Lin J-Y (2015) Cobalt sulfide counter electrodes enhanced by a hydro-thermal treatment for use in platinum-free dye-sensitized solar cells. Mater Res Bull 68:9–15
27. Tai S-Y, Lu M-N, Ho H-P, Xiao Y, Lin J-Y (2014) Investigation of carbon nanotubes decorated with cobalt sulfides of different phases as nanocomposite catalysts in dye-sensitized solar cells. Electrochim Acta 143:216–221
28. Wang G, Zhang J, Kuang S, Liu S, Zhuo S (2014) The production of cobalt sulfide/graphene composite for use as a low-cost counter-electrode material in dye-sensitized solar cells. J Power Sources 269:473–478
29. Jin J, Zhang X, He T (2014) Self-assembled CoS_2 nanocrystal film as an efficient counter electrode for dye-sensitized solar cells. J Phys Chem C 118:24877–24883
30. Chen H-W, Kung C-W, Tseng C-M, Wei T-C, Sakai N, Morita S, Ikegami M, Miyasaka T, Ho K-C (2013) Plastic based dye-sensitized solar cells using Co_9S_8 acicular nanotube arrays as the counter electrode. J Mater Chem A 1:13759
31. Chen C, Ye M, Zhang N, Wen X, Zheng D, Lin C (2015) Preparation of hollow Co_9S_8 nanoneedle arrays as effective counter electrodes for quantum dot-sensitized solar cells. J Mater Chem A 3:6311–6314
32. Sun X, Dou J, Xie F, Li Y, Wei M (2014) One-step preparation of mirror-like NiS nanosheets on ITO for the efficient counter electrode of dye-sensitized solar cells. Chem Commun 50:9869–9871
33. Yang J, Bao C, Zhu K, Yu T, Li F, Liu J, Li Z, Zou Z (2014) High catalytic activity and stability of nickel sulfide and cobalt sulfide hierarchical nanospheres on the counter electrodes for dye-sensitized solar cells. Chem Commun 50:4824–4826
34. Ito S, Murakami TN, Comte P, Liska P, Gratzel C, Nazeeruddin MK, Gratzel M (2008) Fabrication of thin film dye sensitized solar cells with solar to electric power conversion efficiency over 10 %. Thin Solid Films 516:4613–4619
35. Guo W, Chen C, Ye M, Lv M, Lin C (2014) Carbon fiber/Co_9S_8 nanotube arrays hybrid structures for flexible quantum dot-sensitized solar cells. Nanoscale 6:3656–3663
36. Xiao Y, Wang C, Han G (2015) Effects of thiourea concentration on electrocatalytic performances of nickel sulfide counter electrodes for use in dye-sensitized solar cells. Mater Res Bull 61:326–332

37. Pu J, Wang Z, Wu K, Yu N, Sheng E (2014) Co_9S_8 nanotube arrays supported on nickel foam for high-performance supercapacitors. Phys Chem Chem Phys 16:785–791
38. Yin L, Wang L, Liu X, Gai Y, Su L, Qu B, Gong L (2015) Ultrafast microwave synthesis of 3D flower-like Co9S8 hierarchical architectures for high-performance supercapacitor applications. Eur J Inorg Chem 2015:2457–2462
39. http://srdata.nist.gov/xps/Default.aspx (NIST X-ray Photoelectron Spectroscopy Database)
40. Sun P, Yao F, Ban X, Huang N, Sun X (2015) Directly hydrothermal growth of antimony sulfide on conductive substrate as efficient counter electrode for dye-sensitized solar cells. Electrochim Acta 174:127–132
41. Jiang Y, Yu B-B, Liu J, Li Z-H, Sun J-K, Zhong X, Hu J, Song W-G, Wan L-J (2015) Boosting the open circuit voltage and fill factor of QDSSCs using hierarchically assembled ITO@ Cu2S nanowire array counter electrodes. Nano Lett 5:3088–3095
42. Sun W, Peng T, Liu Y, Xu S, Yuan J, Guo S, Zhao X-Z (2013) Hierarchically porous hybrids of polyaniline nanoparticles anchored on reduced graphene oxide sheets as counter electrodes for dye-sensitized solar cells. J Mater Chem A 1:2762–2768
43. Peng T, Sun W, Sun X, Huang N, Liu Y, Bu C, Guo S, Zhao X-Z (2013) Direct tri-constituent co-assembly of highly ordered mesoporous carbon counter electrode for dye-sensitized solar cells. Nanoscale 5:337–341
44. Swami SK, Chaturvedi N, Kumar A, Kapoor R, Dutta V, Frey J, Moehl T, Grätzel M, Mathew S, Nazeeruddin MK (2015) Investigation of electrodeposited cobalt sulphide counter electrodes and their application in next-generation dye sensitized solar cells featuring organic dyes and cobalt-based redox electrolytes. J Power Sources 275:80–89
45. Zheng X, Deng J, Wang N, Deng D, Zhang WH, Bao X, Li C (2014) Podlike N-doped carbon nanotubes encapsulating FeNi alloy nanoparticles: high-performance counter electrode materials for dye-sensitized solar cells. Angew Chem Int Ed Engl 53:7023–7027
46. Koide N, Islam A, Chiba Y, Han L (2006) Improvement of efficiency of dye-sensitized solar cells based on analysis of equivalent circuit. J Photochem Photobiol A 182:296–305
47. Ondersma JW, Hamann TW (2009) Impedance investigation of dye-sensitized solar cells employing outer-sphere redox shuttles. J Phys Chem C 114:638–645
48. Zhao W, Zhu X, Bi H, Cui H, Sun S, Huang F (2013) Novel two-step synthesis of NiS nanoplatelet arrays as efficient counter electrodes for dye-sensitized solar cells. J Power Sources 242:28–32
49. Wang M, Anghel AM, Marsan B, Cevey Ha NL, Pootrakulchote N, Zakeeruddin SM, Grätzel M (2009) CoS supersedes Pt as efficient electrocatalyst for triiodide reduction in dye-sensitized solar cells. J Am Chem Soc 131:15976–15977
50. Dong J, Wu J, Jia J, Wu S, Zhou P, Tu Y, Lan Z (2015) Cobalt selenide nanorods used as a high efficient counter electrode for dye-sensitized solar cells. Electrochim Acta 168:69–75
51. He B, Meng X, Tang Q, Li P, Yuan S, Yang P (2014) Low-cost CoPt alloy counter electrodes for efficient dye-sensitized solar cells. J Power Sources 260:180–185
52. Lin J-Y, Tai S-Y, Chou S-W (2014) bifunctional one-dimensional hierarchical nanostructures composed of cobalt sulfide nanoclusters on carbon nanotubes backbone for dye-sensitized solar cells and supercapacitors. J Phys Chem C 118:823–830